

Original Article

Peptide targeted high-resolution molecular imaging of prostate cancer with MRI

Xueming Wu¹, Guanping Yu¹, Daniel Lindner³, Susann M Brady-Kalnay², Qi Zhang⁴, Zheng-Rong Lu¹

¹Department of Biomedical Engineering, Case Western Reserve University, Cleveland, Ohio 44106, USA; ²Department of Molecular Biology and Microbiology, School of Medicine, Case Western Reserve University, Cleveland, Ohio, USA; ³Department of Translational Hematology & Oncology Research, Cleveland Clinic, Cleveland, Ohio 44195, USA; ⁴Provincial Key Lab of Fine Chemistry, Hainan University, Haikou, China

Received June 18, 2014; Accepted July 15, 2014; Epub September 6, 2014; Published September 15, 2014

Abstract: Non-invasive accurate detection of prostate cancer is critical for clinical management of the disease. Molecular MRI has a potential for accurate detection of prostate cancer with high spatial resolution. Fibronectin is a hallmark of epithelial-mesenchymal transition occurred in aggressive prostate cancer and highly expressed in malignant tumors. A pentapeptide CREKA targeted contrast agent CREKA-dL-(DOTA-Gd)₄ was synthesized and evaluated to target fibrin-fibronectin complexes in tumor extracellular matrix for molecular MRI of prostate cancer. The contrast agent was synthesized by solid-phase peptide synthesis. The T₁ relaxivity of CREKA-(DOTA-Gd)₄ at 1.5 T was 33.2 mM⁻¹s⁻¹ per molecule (8.3 per Gd). The fluorescence imaging showed that CREKA specifically bound to orthotopic PC3 prostate tumor in athymic nude mice. Strong enhancement was observed in the tumor tissue injected with CREKA-(DOTA-Gd)₄ in the first 5 minutes post-injection before MR signal became visible in the bladder at a low dose of 0.03 mmol-Gd/kg. The targeted contrast agent exhibited minimal Gd retention in the main organs and tissues 2 days after injection. The peptide targeted contrast agent CREKA-(DOTA-Gd)₄ is promising for high-resolution molecular MRI of prostate cancer.

Keywords: Molecular imaging, MRI, prostate cancer, peptide, targeted contrast agent

Introduction

Prostate cancer is the most common noncutaneous malignancy with an estimated quarter million men who are diagnosed with prostate cancer through prostate specific antigen (PSA) screening every year in the United States [1]. The current diagnostic strategy combining PSA level and Gleason grade from the standard 12-core prostate needle-biopsy does not accurately determine prostate cancer aggressiveness and risk [2-4]. This inaccuracy stems from multifocal nature of prostate cancer, co-existence of various grades of cancer within the same prostate, inadequate prostate sampling from needle-biopsy, and difficulty of assigning accurate Gleason grade to the minute size of cancer in the needle-biopsy specimens. Consequently, most patients will receive treatment even for low risk disease to avoid potential undertreatment, which may lead to the treatment-related long-term side effects. In

fact, there is about 20% or higher risk of upgrading the score after radical prostatectomy when compared with the original Gleason grade from the biopsy specimen. Accurate detection and differential diagnosis of prostate cancer are essential for the clinical management and treatment of aggressive prostate cancer.

Various diagnostic strategies have been proposed to improve the accuracy of prostate cancer detection, diagnosis and risk assessment, including medical imaging such as multiparametric MRI [5-9]. Molecular imaging of the biomarkers associated with prostate cancer aggressiveness will be a valuable tool for detection, differential diagnosis and prognosis of prostate cancer. It can be used to accurately, non-invasively and molecularly determine the altered expression of the biomarkers in the entire prostate for more accurate diagnosis and prognosis than currently used diagnostic tools.

An MRI contrast agent for prostate cancer imaging

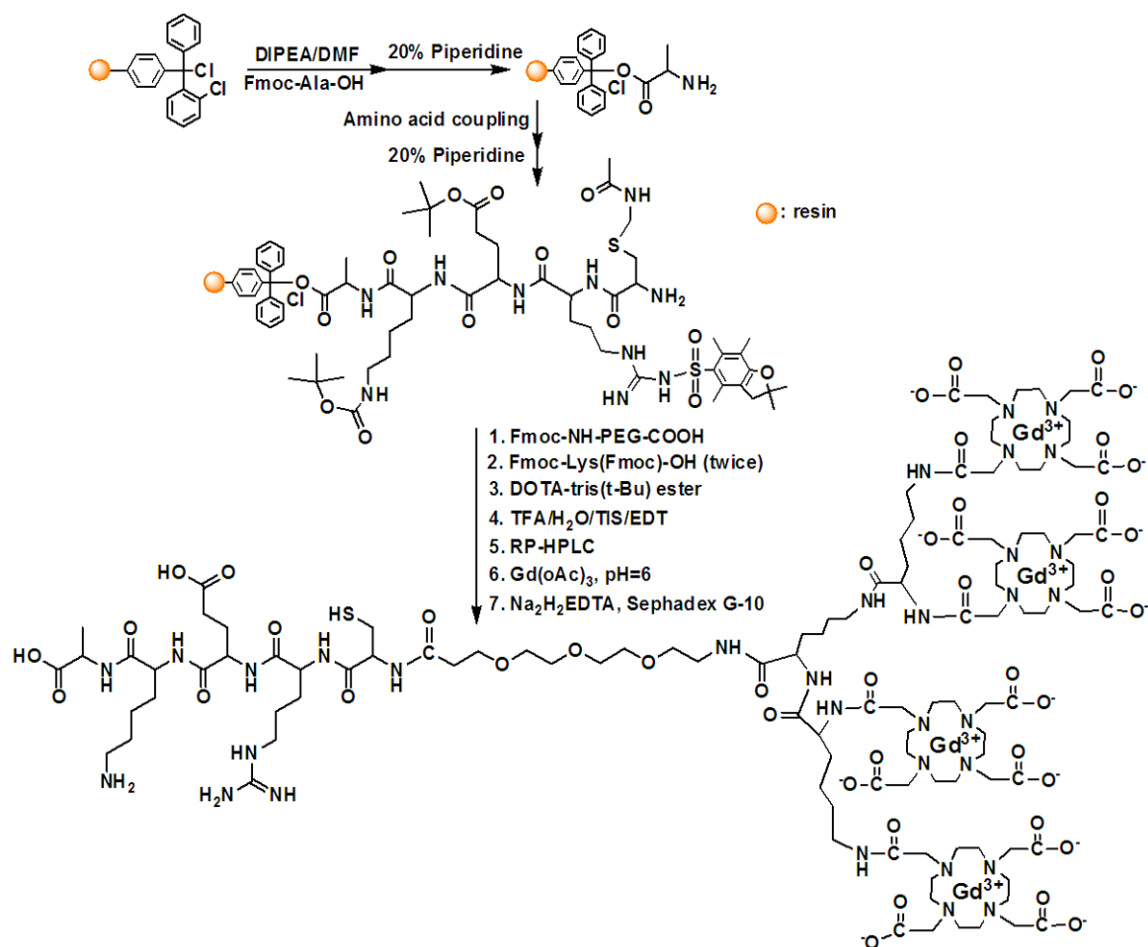


Figure 1. Synthesis of CREKA-dL-(Gd-DOTA)₄.

Fibronectin (FN) is a glycoprotein that forms extracellular matrix via a complexation with other extracellular matrix components, including collagen and fibrin. Altered fibronectin expression, degradation, and organization are associated with a number of pathologies, including cancer [10, 11]. It is one of the hallmarks of epithelial-to-mesenchymal transition (EMT) and plays a key role in EMT induction [12]. EMT is considered as a biological process that facilitates the progression and metastasis of many malignant human cancer types, including prostate cancer [13-16]. Several studies have shown that fibronectin is highly expressed in prostate cancer, while there is a very low expression in benign lesions, including BPH [17-20]. The presence of fibronectin in the extracellular matrix of advanced human cancer promotes tumor angiogenesis, proliferation and metastasis. Highly expressed fibronectin and its complexes with other matrix protein can be viable biomarkers for molecular imaging of prostate cancer.

Previously, we synthesized and evaluated a small peptide targeted MRI contrast agent, CLT1-dL-(Gd-DOTA)₄ [21], for prostate cancer imaging. CLT1 (CGLIIQKNEC) peptide specifically binds to fibrin-fibronectin complexes in tumor extracellular matrix for tumor homing [22]. CLT1-dL-(Gd-DOTA)₄ was effective for molecular MRI of prostate cancer in an orthotopic mouse tumor model. However, it suffered from various limitations for further development, including relatively high tissue retention after the imaging due to the poor water solubility of CLT1 peptide. Further structural modification is needed to address the limitations of the small molecular targeted MRI contrast agents for prostate cancer imaging.

In this study, we synthesized and evaluated a new low molecular weight CREKA targeted contrast agent CREKA-dL-(Gd-DOTA)₄ using generation 1 lysine dendrimer for molecular MRI of prostate cancer. CREKA is a small peptide that

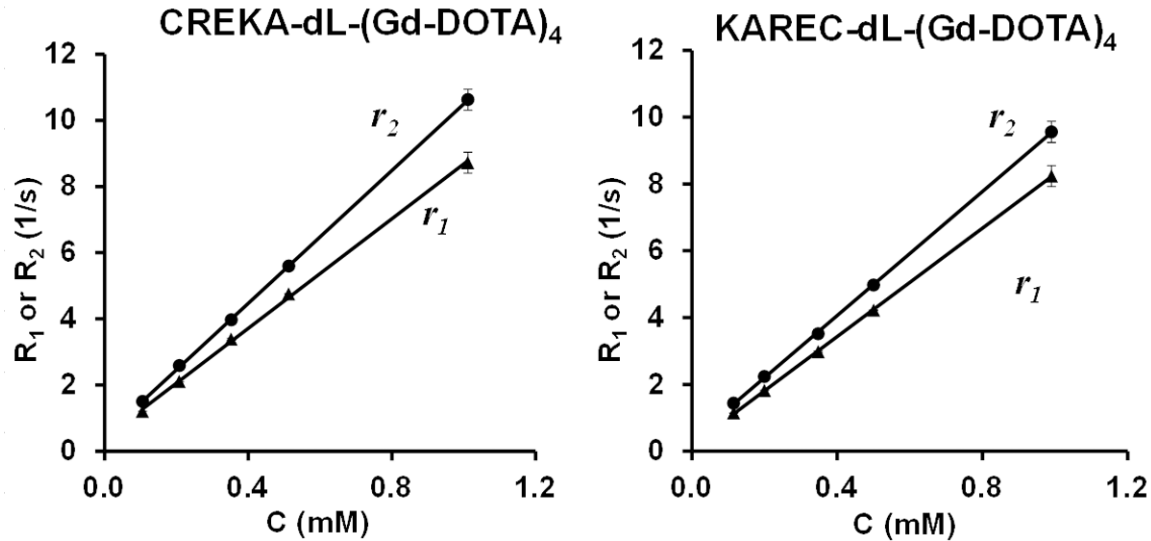


Figure 2. Plots of R_1 ($1/T_1$) and R_2 ($1/T_2$) versus the Gd(III) concentration of CREKA-dL-(Gd-DOTA)₄ and KAREC-dL-(Gd-DOTA)₄.

Table 1. Relaxivities of the targeted and scrambled MRI contrast agents measured at 37 °C, pH 7.4 and 1.5T

	r_1 (mM ⁻¹ .s ⁻¹)		r_2 (mM ⁻¹ .s ⁻¹)		Gd content (mmol-Gd/g)
	per Gd	per molecule	per Gd	per molecule	
CREKA-dL-(Gd-DOTA) ₄	8.3 ± 0.4	33.2 ± 1.6	10.1 ± 0.3	40.4 ± 1.2	1.07 ± 0.18
KAREC-dL-(Gd-DOTA) ₄	8.1 ± 0.2	32.4 ± 0.8	9.3 ± 0.5	37.2 ± 2.0	1.04 ± 0.10
Gd-DOTA	2.9*	2.9*	3.2*	3.2*	-

*Relaxivities for Gd-DOTA in water at 37 °C are from reference [24].

specifically binds to the fibronectin-fibrin complexes in tumor ECM [23] and has good water solubility. A corresponding scrambled targeted agent KAREC was synthesized and used as a non-targeted control agent. We first assessed the physicochemical properties of the targeted contrast agent. The tumor specificity of CREKA was determined in an orthotopic xenograft PC3 prostate tumor model in male athymic nude mice using fluorescence imaging. The effectiveness of CREKA-dL-(Gd-DOTA)₄ for MR molecular imaging of the prostate tumor was determined in the same tumor model. The tissue retention of the contrast agents was determined in the animal model.

Materials and methods

Experimental section

Fmoc protected amino acids Fmoc-Ala-OH, Fmoc-Lys(Boc)-OH, Fmoc-Glu(OtBu)-OH, Fmoc-Arg(Pbf)-OH, Fmoc-Cys(trt)-OH and Fmoc-12-amino-4,7,10-trioxadodecanoic acid (Fmoc-NH-

PEG-COOH, MW = 443.5) were purchased from EMD Chemicals Inc. (Gibbstown, NJ, USA). 1,4,7,10-Tetraazacyclododecane-1,4,7-tris-*tert*-butyl acetate-10-acetic acid [DOTA-tris(*t*-Bu)] was purchased from TCI America (Portland, OR, USA). Benzotriazol-1-yl-oxytripyrrolidinophosphonium hexafluorophosphate (PyBOP), 1-hydroxybenzotriazole hydrate (HOBt), and 2-(1*H*-benzotriazol-1-yl)-1,1,3,3-tetramethyl uronium hexafluorophosphate (HBTU) were purchased from Nova Biochem (Darmstadt, Germany). Triisobutylsilane (TIS) and 1,2-ethanedithiol (EDT) were purchased from Sigma-Aldrich Corp. (St. Louis, MO, USA). Texas Red succinimidyl ester (T20175) was purchased from Invitrogen (Eugene, Oregon, USA). Anhydrous *N,N*-diisopropylethylamine (DIPEA), dichloromethane, and *N,N*-dimethylformamide (DMF) were purchased from Alfa Aesar (Ward Hill, MA, USA). Trifluoroacetic acid (TFA) was purchased from ACROS Organics (Morris Plains, NJ, USA). All reagents were used without further purification.

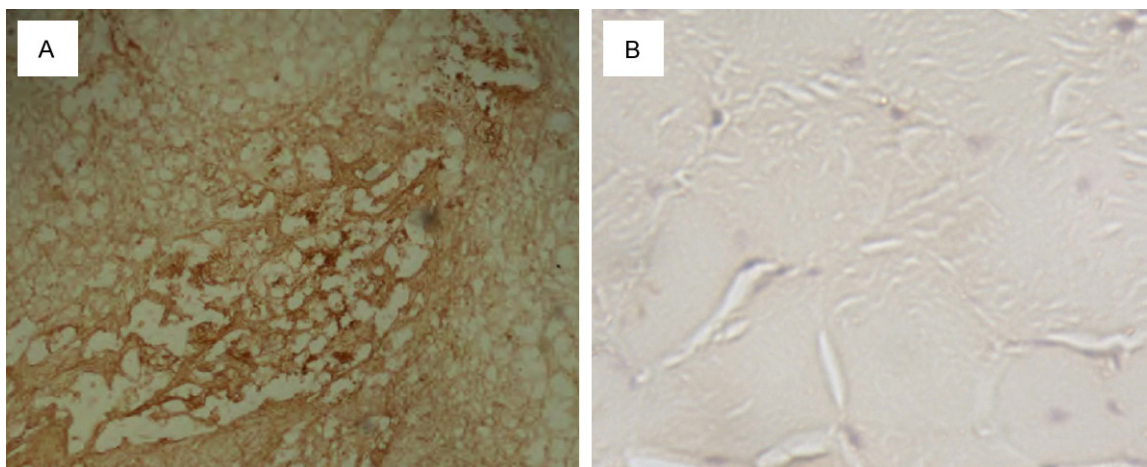


Figure 3. (A) Immunohistochemical staining of fibronectin in PC3 tumor tissue (A) and normal mouse muscle (B).

Synthesis of CREKA-dL-(Gd-DOTA)₄ and KAREC-dL-(Gd-DOTA)₄

Peptide CREKA was synthesized using a standard Fmoc solid phase peptide synthetic chemistry on a 2-chlorotrityl chloride resin. After conjugating a PEG spacer to the peptide on the resin in the presence of coupling agents, an N_α,N_ε-Fmoc protected lysine was then conjugated to the amino group of PEG followed by Fmoc removal and the conjugation of two more N_α,N_ε-Fmoc protected lysine residues to the amino groups of the lysine on the resin. After removal of Fmoc protecting groups, a twofold excess (relative to the resin bound amine groups) of the DOTA-tris(t-butyl ester) was reacted with the 4 amino groups of the lysine residues of each targeting moiety on the resin in the presence of HBTU/HOBt/DIPEA for 2 h. Then the peptide-dL-(DOTA)₄ ligand was removed and completely deprotected from the resin by treating with an acid cocktail of TFA:water:TIS:EDT (95:2:1:2) for 8 h. The CREKA-dL-(DOTA)₄ ligand was purified by high performance liquid chromatography (HPLC) on an Agilent 1100 HPLC system equipped with a ZORBAX 300SB-C18 PrepHT column. The gradient of eluents was 0-40% solvent B (0.1% TFA in acetonitrile) in solvent A (0.1% TFA aqueous solution) for 20 min and 40-90% solvent B in solvent A for 10 min. The pure ligand was chelated with Gd(III) by reacting with Gd(OAc)₃ at pH 6 for 2 days at room temperature. A slight excess of Gd(OAc)₃ was used to ensure complete chelation. The excess Gd³⁺ was removed with EDTA, and the product is then purified by

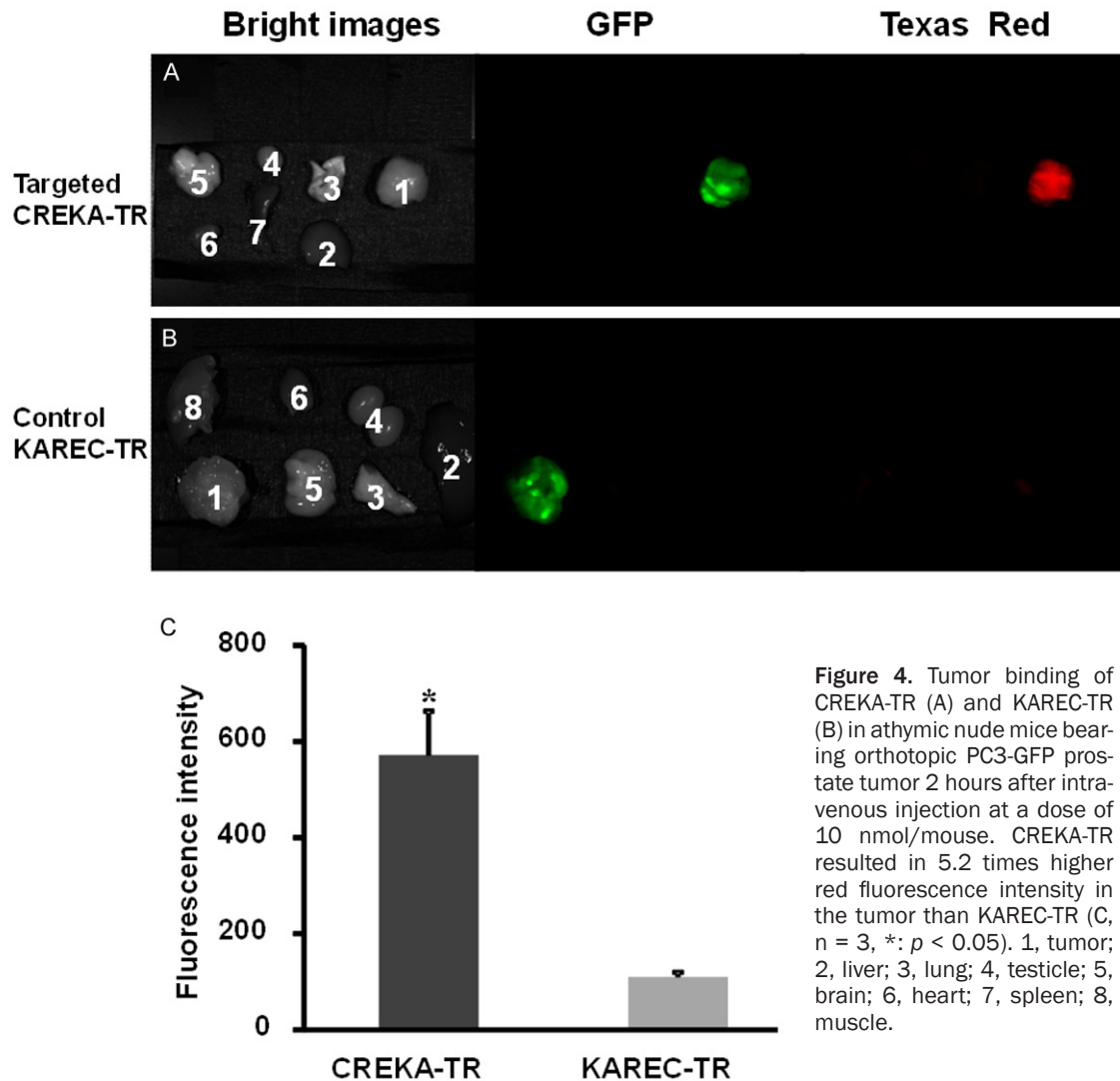
Sephadex G-10 column to give final product CREKA-dL-(Gd-DOTA)₄, as shown in **Figure 1**. MALDI-TOF (*m/z*, [M+H]⁺): 3355.16 (obsd.); 3355.97 (calcd.). Scrambled agent KAREC-dL-(Gd-DOTA)₄ was synthesized using the same procedure. The final product KAREC-dL-(Gd-DOTA)₄ was also characterized by MALDI-TOF (*m/z*, [M+H]⁺): 3355.05 (obsd.); 3355.97 (calcd.).

Synthesis of CREKA-Texas Red (TR) and scrambled KAREC-TR conjugates

The peptides CREKA and KAREC were synthesized using standard solid-phase peptide chemistry. Texas Red (2 mg) was then conjugated to the peptides on resin (10 mg) in the presence of coupling agents. After cleaved from the resin with an acidic cocktail of TFA:water:TIS:EDT (95:2:1:2), the crude products CREKA-TR and KAREC-TR were purified by preparative HPLC. Molecular weight of the conjugates was determined by MALDI-TOF mass spectrometry, CREKA-TR (*m/z*, [M+H]⁺): 1510.29 (obsd.), 1510.80 (calcd.); KAREC-TR: (*m/z*, [M+H]⁺): 1510.32 (obsd.).

Characterization of the contrast agents

The Gd(III) content was measured by inductively coupled plasma-optical emission spectroscopy (ICP-OES Optima 3100XL, Perkin-Elmer, Norwalk, CT). MALDI-TOF mass spectra were acquired on a MALDI-TOF mass spectrometer (AutoflexTM Speed, Bruker) in a linear mode with 2,5-dihydroxybenzoic acid (2,5-DHB) as a matrix. Relaxation times of the aqueous solu-



tion of CREKA-dL-(Gd-DOTA)₄ or KAREC-dL-(Gd-DOTA)₄ with different concentrations were measured at 60 MHz (1.5 T) using a Bruker minispec relaxometer at 37°C. T_1 was measured with an inversion-recovery pulse sequence. T_2 was measured using a Carr-Purcell-Meiboom-Gill sequence with 500 echoes collected. The T_1 and T_2 relaxivities of the agents were calculated from the slopes of the plots of $1/T_1$ and $1/T_2$ versus the Gd concentrations.

Animal model

Male NIH athymic nude mice were maintained at the Athymic Animal Core Facility at Case Western Reserve University according to an animal protocol approved by the CWRU Institutional Animal Care and Use Committee. PC3 prostate cancer cells with constitutive expression of green fluorescence protein (GFP)

were cultured in RPMI medium supplemented with 5% fetal bovine serum and penicillin/streptomycin/fungizone, harvested by trypsinization and resuspended at a density of 2.5×10^4 cells per 1.0 μ L PBS. The mice were anesthetized and a small incision was made through the skin and peritoneum along the lower midline for about 1 cm. The prostate dorsal lobes were gently exteriorized and stabilized. The suspension of PC3-GFP cells in PBS (10 μ L) was injected into the prostate using a 30-gauge needle. Finally the incision was closed with wound autoclip [23]. Tumor growth in the mice was monitored by GFP fluorescence imaging on a Maestro fluorescence imager.

Immunohistochemical studies

Mice were sacrificed for immunohistochemical studies. The tumor tissue and normal muscle

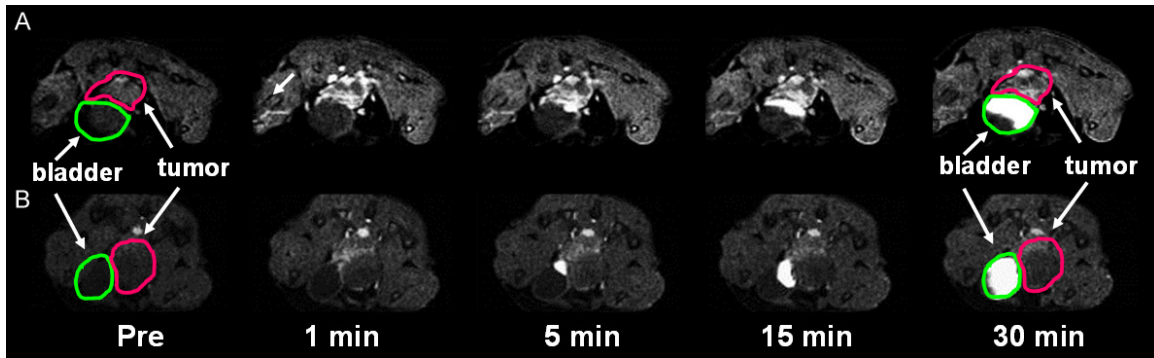


Figure 5. Representative T_1 -weighted axial 2D MR images of orthotopic PC-3 human prostate tumor before and at different time points after intravenous injection of CREKA-dL-(Gd-DOTA)₄ (A) and KAREC-dL-(Gd-DOTA)₄ (B) at 0.03 mmol-Gd/kg in nu/nu nude mice.

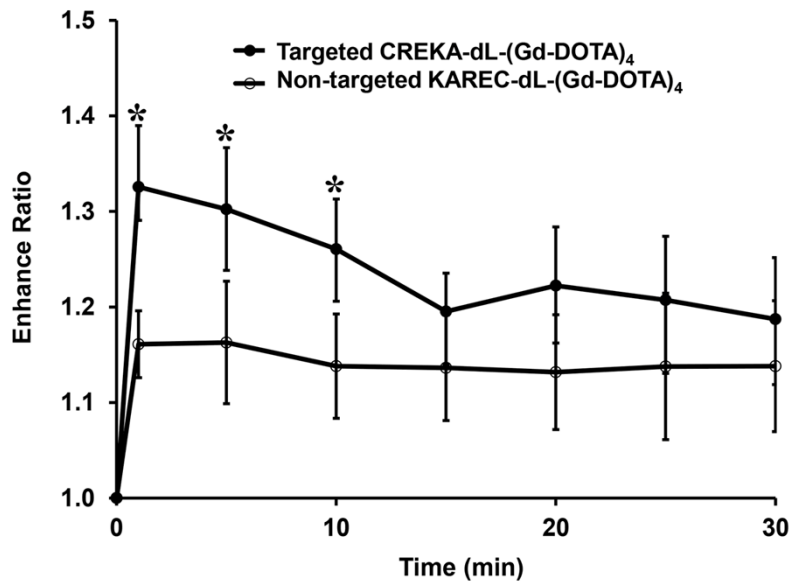


Figure 6. Tumor enhancement ratio of CREKA-dL-(Gd-DOTA)₄ and KAREC-dL-(Gd-DOTA)₄ at 0.03 mmol-Gd/kg in nu/nu nude athymic mice (n = 6) bearing orthotopic human prostate tumor.

were excised and fixed with 4% paraformaldehyde, then embedded in optimum cutting temperature (OCT) compounds. The sliced tumor or normal muscle tissue sections with 5 μ m thickness were fixed with pre-cooled fixative (acetone) for 5-10 min, and were incubated in 3% H₂O₂/MeOH for 30 minutes at room temperature to block endogenous peroxidase activity, incubated in 10% normal goat serum (NGS) in TBS for 30 min to block nonspecific binding. The sections were then incubated overnight at 4°C with primary antibodies at appropriate dilutions (rabbit polyclonal to fibronectin, mouse monoclonal [UC45] to fibrin alpha chain, Abcam). After washing with PBS, blocked with

10% NGS in TBS for 10 min, the secondary antibody (goat anti-rabbit IgG (H+L), horseradish peroxidase conjugate, Abcam) was applied for 30 min and the signals visualized using 0.75 mg/ml 3,3'-diaminobenzidine (DAB) with 0.015% hydrogen peroxide in Tris buffer. (DAB/DAB+ Chromogen Solution, Dako).

Tumor fluorescence imaging

Texas Red labeled peptides were intravenously injected to the tumor bearing mice at a dose of 10 nmol/mouse. After 2 h, the mice were sacrificed, and the tumors and major organs were collected and imaged immediately on a Maestro fluorescence

imager. Fluorescence images were obtained using green light filters for GFP (excitation: 444-490 nm; emission: 515 nm long-pass filter; acquisition settings: 500-720 in 10 nm steps) and red light filters for Texas Red labeled probes (excitation: 576-621 nm; emission: 635 nm long-pass filter; acquisition settings: 630-800 in 10 nm steps). Exposure time was 10 ms for GFP and 100 ms for Texas Red.

Tumor MRI

The MRI study was performed on a Bruker Biospec 7 T MRI scanner (Bruker Corp., Billerica, MA, USA) with a volume radio frequen-

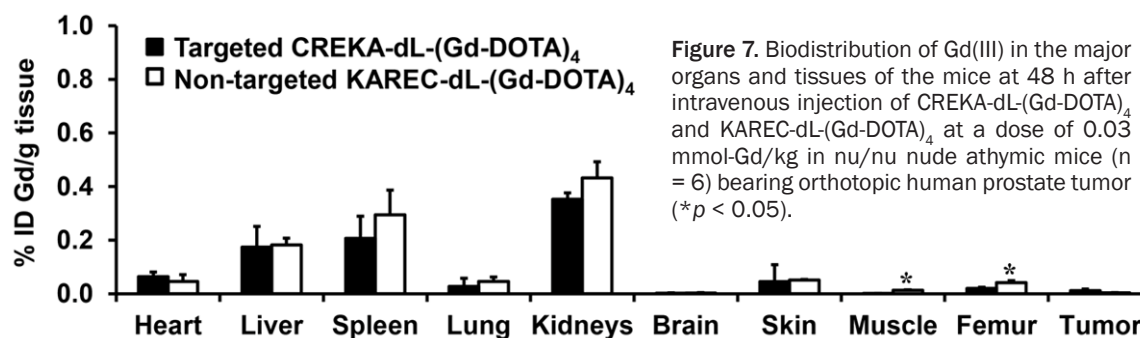


Figure 7. Biodistribution of Gd(III) in the major organs and tissues of the mice at 48 h after intravenous injection of CREKA-dL-(Gd-DOTA)₄ and KAREC-dL-(Gd-DOTA)₄ at a dose of 0.03 mmol-Gd/kg in nu/nu nude athymic mice (n = 6) bearing orthotopic human prostate tumor (**p* < 0.05).

cy (RF) coil. Mice were anesthetized with a 2% isoflurane-oxygen mixture in an isoflurane induction chamber. A tail vein of mouse was catheterized with a 30 gauge needle connected with a 2.5 m long tubing filled with heparinized saline. The animal was then placed into the magnet and kept under inhalation anesthesia with 1.5% isoflurane-oxygen via a nose cone. A respiratory sensor connected to a monitoring system (SA Instruments, Stony Brook, NY) was placed on the abdomen to monitor rate and depth of respiration. The body temperature was maintained at 37°C by blowing hot air into the magnet through a feedback control system. A group of 6 mice was used for each agent. Sagittal section images were acquired with a localizing sequence to identify the tumor location, followed by a 2D T_1 -weighted gradient fat suppression sequence before injection. After pre-injection baseline MR image acquisition, the targeted agent or control agent was injected at a dose of 0.03 mmol of Gd/kg by flushing with 200 μ L of saline. T_1 -weighted 2D axial images were then acquired at different time points after the injection for up to 30 min. Parameters of the 2D T_1 -weighted gradient echo sequence were TR/TE = 151.2/1.9 ms, FOV = 3.0 cm, slice thickness = 1.2 mm, slice number = 12, average = 1, flip angle = 80°, matrix = 128×128.

Image analysis was performed by using Bruker ParaVision 4.0 imaging software. Regions of interest (ROIs) were drawn over the whole tumor in the two-dimensional imaging plane and average signal intensity was measured in the ROIs. Enhancement ratio (ER) was calculated using the following equations: $ER = (S_t - S_0) / S_0$, where S_t and S_0 denoted the signal in tumor before and after contrast injection. The *p* values were calculated using the student's two-

tailed *t*-test, assuming statistical significance at *p* < 0.05.

Biodistribution study

The mice from the MRI study were sacrificed by cervical dislocation at 48 h post-injection. The organ and tissue samples, including the heart, liver, spleen, lung, kidneys, brain, skin, muscle, femur, and tumor were collected and weighed. The tissue samples were then cut into small pieces and mixed with ultra-pure nitric acid (1.0 ml, 70%, EMD, Gibbstown, NJ). The tissue samples were liquefied for 1 week, and the solution was transferred to a centrifuge tube and centrifuged at 14,000 rpm for 5 min. The supernatant (0.2 ml) was diluted 10 times with de-ionized water and further centrifuged at 14,000 rpm for 5 min. The Gd(III) concentration in the supernatant solution was measured by ICP-OES. The average Gd(III) content in each organ or tissue was calculated from the measured Gd(III). The Gd content was calculated as the percentage of injected dose per gram of tissues (% ID/g).

Results

Synthesis and characterization

CREKA-dL-(Gd-DOTA)₄ consists of a 5 amino acid peptide for targeting fibrin-fibronectin complexes in tumor and four Gd-DOTA mono-amide chelates for MRI signal enhancement. A generation 1 lysine dendrimer was used to increase the molar ratio of Gd-DOTA mono-amide to the peptide in the targeted contrast agent for effective targeted contrast enhancement. A short PEG spacer was used in between the peptide and lysine dendrimer to avoid steric hindrance of the chelates for target binding. The synthesis of CREKA-dL-(Gd-DOTA)₄ is described in **Figure 1**. The total yield of peptide

CREKA-dL-(Gd-DOTA)₄ and KAREC-dL-(Gd-DOTA)₄ was 38.2% and 33.5% after purification. The structure of CREKA-dL-(Gd-DOTA)₄ and KAREC-dL-(Gd-DOTA)₄ was confirmed by MALDI-TOF mass spectrometry. **Figure 2** shows the plots of the T_1 and T_2 water proton relaxation rates versus the concentration of CREKA-dL-(Gd-DOTA)₄ and KAREC-dL-(Gd-DOTA)₄ at 1.5 T (60 MHz), 37°C. The physicochemical parameters of the contrast agents are listed in **Table 1**. Both targeted and scrambled agents had similar relaxivity values. At 1.5 T, the T_1 relaxivity per gadolinium of CREKA-dL-(Gd-DOTA)₄ in pH 7.4 PBS was about twice higher than that of Gd-DOTA [24].

Immunohistochemical studies

Immunohistochemical analysis using an anti-fibronectin antibody confirmed the presence of the elevated fibronectin expression in the tumor tissue. **Figure 3** shows the immunohistochemical staining of fibronectin in tumor and normal muscle specimens. The staining clearly indicated the existence of fibronectin in extracellular spaces of tumor tissue, not in the normal muscle tissue.

Tumor binding of CREKA peptide

Binding specificity of CREKA to prostate tumor was determined using fluorescence imaging in mice bearing orthotopic PC3-GFP prostate tumor. **Figure 4** shows the bright-field images and fluorescence images of tumors and major organs after the mice were sacrificed 2 hours after the injection with CREKA-TR and KAREC-TR. The tumor was labeled with GFP and showed strong green fluorescence. Strong fluorescence was observed in the tumor, not in other tissues and organs from the mice injected with Texas Red labeled CREKA, indicating specific tumor binding of CREKA. KAREC-TR showed little binding in both normal tissues and tumor tissues. Red fluorescence intensity was measured in the orthotopic prostate tumors of the mice injected with CREKA-TR and KAREC-TR. CREKA-TR showed 5.2 times higher binding to the tumor tissue than the control KAREC-TR, **Figure 4C**.

MR molecular imaging of prostate cancer

Figure 5 shows the representative dynamic T_1 -weighted axial 2D MR images of the ortho-

topic human prostate tumor in male nu/nu athymic mice (n = 6) contrast enhanced with CREKA-dL-(Gd-DOTA)₄ and control KAREC-dL-(Gd-DOTA)₄ at 0.03 mmol-Gd/kg. Strong tumor enhancement was observed within first five minutes after injection of CREKA-dL-(Gd-DOTA)₄ and the enhancement lasted for at least 30 minutes. In comparison, the non-targeted control showed little tumor enhancement throughout the experiment. **Figure 6** shows the signal enhancement ratio (ER) in the tumor tissue (the ratio of signal intensity after contrast to that before contrast) up to 30 min after injection. CREKA-dL-(Gd-DOTA)₄ resulted in approximately 108% more signal enhancement than KAREC-dL-(Gd-DOTA)₄ in the tumor tissue at 1 minute post-injection. Although the tumor enhancement with the targeted agent gradually decreased over time, it had still about 58% more signal than the control agent at 30 minutes post-injection. CREKA-dL-(Gd-DOTA)₄ produced more significant signal enhancement in the tumor tissue than the control agent ($p < 0.05$) for at least 10 minutes. Strong contrast enhancement was observed in the urinary bladder 5 minutes after the injection of both agents and contrast enhancement in the urinary bladder gradually increased over time, indicating that the unbound contrast agents were excreted via renal filtration.

Biodistribution in mice

Figure 7 shows the retention of Gd(III) in the major organs and tissues, including the femur, heart, kidneys, liver, lung, muscle, and spleen, 48 h after injection of CREKA-dL-(DOTA-Gd)₄ and KAREC-dL-(DOTA-Gd)₄. Both agents had comparable Gd retention ($p > 0.05$) in the normal organs and tissues 48 hours after the injection. Approximately 0.17%, 0.21% and 0.35% of injected targeted CREKA-dL-(DOTA-Gd)₄ per gram of tissue was measured in the liver, spleen and kidneys, while very little (less than 0.05%) or no Gd was measured in other tissues and organs. Gd(III) tissue retention with these agents was much lower than CLT1-dL-(Gd-DOTA)₄ in our previous report [21].

Discussion

MRI is a clinical imaging modality that provides high-resolution three-dimensional anatomic images of soft tissues. Current clinical contrast agents are mostly non-specific agents and not

able to measure the alteration of cancer biomarkers for molecular cancer imaging. Contrast enhanced MRI with a safe and effective targeted contrast agent has a potential for detecting human prostate cancer with high spatial resolution. Innovative design and development of targeted MRI contrast agents would greatly advance the application of molecular MRI for prostate cancer detection and diagnosis. Two main aspects should be considered in the design and development of targeted MRI contrast agents, the cancer-related biomarkers and the structure of the targeted agents that bind to the biomarkers. Previous efforts on designing targeted MRI contrast agents are mostly focused on targeting the biomarkers on the surface of cancer cells. Due to relatively low sensitivity of MRI and low concentration of the biomarkers on cancer cell surface, little success has yet been achieved to generate sufficient contrast enhancement for effective cancer molecular imaging. In order to obtain sufficient signal enhancement, various delivery systems such as liposomes, colloids, nanoparticles and polymer conjugates with high payload of contrast agents have been developed to increase local concentration of the agents at the target sites [25-28]. Although these delivery systems are effective for tumor MRI in animal models, their slow and incomplete elimination due to their big sizes and consequent release and accumulation of toxic Gd(III) ions in the body may cause potential toxic side effects, such as nephrogenic systemic fibrosis [29, 30]. Clinical development and application of targeted MRI contrast agents with large sizes is hindered by these safety concerns [31-33].

We have recently explored a new strategy for cancer molecular MRI by targeting the cancer-related extracellular matrix proteins, fibrin-fibronectin complexes, using small molecular peptide targeted Gd(III) chelates [34, 35]. We have designed and synthesized CLT1 peptide targeted Gd(III) chelate, CLT1-dL-(Gd-DOTA)₄ for molecular MRI of prostate cancer [21]. CLT1 peptide (CGLIIQKNEC) was first reported by Ruoslahti's group for plasma fibrin-fibronectin clots in solid tumors [22]. The biomarker was abundant in the tumor extracellular matrix and allowed the binding of a sufficient amount of the targeted contrast agent for effective molecular MRI of prostate cancer in an orthotopic mouse model. Unfortunately, the cyclic deca-

peptide with a disulfide bond was highly hydrophobic and CLT1-dL-(Gd-DOTA)₄ had poor water solubility, not suitable for clinical development. Pentapeptide CREKA was another tumor homing peptide specific to clotted plasma proteins (fibrin-fibronectin complexes) formed in tumor stroma [36]. Previous studies have confirmed the tumor binding specificity of CREKA peptide in different types of animal tumor models, including syngeneic B16F1 melanoma tumors in nude mice, xenograft MDA-MB-435 human breast cancer in Balb/c nude mice, and spontaneous MMTV-PyMT breast cancer in transgenic MMTV-PyMT mice [37], and mouse 4T1 breast cancer [38]. In this study, we tested the effectiveness of a CREKA targeted small molecular contrast agent for prostate cancer molecular MRI.

Synthesis of CREKA-dL-(Gd-DOTA)₄ is more convenient than that of CLT1-dL-(Gd-DOTA)₄ with less steps and higher yield. CREKA-dL-(Gd-DOTA)₄ possessed excellent water solubility and much higher relaxivities than a macrocyclic clinical agent Gd-DOTA. Its T₁ relaxivity was slightly lower than that of CLT1-dL-(Gd-DOTA)₄, possibly due to poor water-solubility and slightly large size of the latter. CREKA exhibited high binding specificity in prostate tumor. The combination of high T₁ relaxivity and specific tumor binding would allow effective contrast enhanced cancer MRI at a reduced dose.

CREKA-dL-(Gd-DOTA)₄ produced strong enhancement in the MR images of the orthotopic prostate tumor at 0.03 mmol-Gd/kg, a significantly reduced dose as compared to that (0.1 mmol/kg) of commonly used clinical Gd(III) based agent. The tumor enhancement was clearly visible in the first 5 minutes before the contrast agent accumulated in the bladder, while the non-targeted control agent did not produce significant signal enhancement in prostate tumor. Strong bladder contrast enhancement after the renal clearance of the contrast agent could interfere diagnostic imaging of the prostate cancer. Strong enhancement became visible in the bladder at 15 minutes after contrast injection. The targeted contrast agent was able to produce strong tumor enhancement before its clearance in the bladder. The time window for effective contrast enhancement in the tumor without the interference from the bladder is critical to accurate

detection of prostate cancer. The high expression of fibrin-fibronectin complexes in the tumor model enabled the binding of a sufficient amount of small molecular targeted contrast agent to generate strong signal enhancement for effective molecular MRI of prostate cancer.

We have further demonstrated in this study that molecular MRI of an abundant cancer biomarker in tumor extracellular matrix with a small molecular targeted contrast agent is effective for high-resolution molecular imaging of prostate cancer. Since human prostate cancer is heterogeneous and multifocal in nature, high-resolution molecular MRI of prostate cancer has a potential to detect all tumors in the prostate. Nuclear medicine is a commonly used imaging modality for cancer molecular imaging. However, it might be challenging to detect and localize multifocal tumors within the prostate with nuclear medicine due to its poor spatial resolution for cancer imaging. Molecular MRI can overcome the limitation of nuclear medicine to achieve high-resolution of molecular imaging of prostate tumors.

Safety is the key parameter for clinical development and application of MRI contrast agents. The toxicity of free Gd(III) ions is the major safety concern for Gd(III) based MRI contrast agents, especially for patients with kidney function failure diseases. High chelation stability and complete elimination of the Gd(III) based MRI contrast agents from the body are essential for alleviating the safety concerns. Macrocyclic chelate Gd-DOTA and its derivatives have high chelate stability. We have shown that Gd-DOTA monoamide is highly stable against transmetallation with no release of toxic Gd(III) ions with the presence of endogenous metal ions, such as Zn^{2+} [39]. Gd-DOTA monoamide has been used in the peptide targeted contrast agent to avoid any potential release toxic Gd(III) ions *in vivo*. The small size and good water solubility of CREKA-dL-(Gd-DOTA)₄ facilitate diffusion into tumor tissues and effective binding to the biomarkers, and rapid clearance of unbound agent from the circulation. Rapid clearance of the unbound agent reduces background signal, minimizes the accumulation of Gd(III) chelates in the body, and alleviates potential pharmacological effects from the peptide in the targeted contrast agent. Consequently, CREKA-dL-(Gd-DOTA)₄ had minimal Gd retention in the main

organs and tissues 2 days after injection, much lower than CLT1-dL-(Gd-DOTA)₄. High chelation stability and minimal tissue retention are the advantageous safety features of CREKA-dL-(Gd-DOTA)₄ for further clinical development for detection and diagnosis of prostate cancer.

Conclusion

In summary, we synthesized and evaluated CREKA-dL-(Gd-DOTA)₄ as a small molecular targeted contrast agent with improved physicochemical and pharmaceutical properties for molecular MRI of prostate cancer. The contrast agent possessed good water solubility and high relaxivities. CREKA-dL-(Gd-DOTA)₄ was effective for specific tumor imaging at a reduced dose (0.03 mmol/kg). It produced strong tumor contrast enhancement for at least 5 minutes before the signal enhancement in the bladder became visible. The unbound contrast agents had minimal tissue retention at 48 hours after injection. CREKA-dL-(Gd-DOTA)₄ possessed several advantages, including simple structure, small size for rapid renal filtration, good water solubility, high relaxivity, tumor specificity and good safety profile. CREKA-dL-(Gd-DOTA)₄ is promising for high-resolution molecular imaging and detection of prostate cancer with MRI.

Acknowledgements

This work is supported in part an NIH grant R01 EB000489 and a grant (KJHZ2014-05) from the International Science and Technology Cooperation Projects of Hainan Province, China.

Address correspondence to: Dr. Zheng-Rong Lu, Department of Biomedical Engineering, Case Western Reserve University, Room 427, Wickenden Building, 10900 Euclid Avenue, Cleveland, OH 44106-7207. E-mail: zxl125@case.edu

References

- [1] Siegel R, Naishadham D and Jemal A. Cancer statistics, 2013. *CA Cancer J Clin* 2013; 63: 11-30.
- [2] Shah RB. Current perspectives on the Gleason grading of prostate cancer. *Arch Pathol Lab Med* 2009; 133: 1810-1816.
- [3] Mehta V, Rycyna K, Baesens BM, Barkan GA, Paner GP, Flanigan RC, Wojcik EM and Venkataraman G. Predictors of Gleason Score (GS) upgrading on subsequent prostatectomy:

- a single Institution study in a cohort of patients with GS 6. *Int J Clin Exp Pathol* 2012; 5: 496-502.
- [4] Heijnsdijk EA, der Kinderen A, Wever EM, Draisma G, Roobol MJ and de Koning HJ. Overdetection, overtreatment and costs in prostate-specific antigen screening for prostate cancer. *Br J Cancer* 2009; 101: 1833-1838.
 - [5] Durmus T, Reichelt U, Huppertz A, Hamm B, Beyersdorff D and Franiel T. MRI-guided biopsy of the prostate: correlation between the cancer detection rate and the number of previous negative TRUS biopsies. *Diagn Interv Radiol* 2013; 19: 411-417.
 - [6] Turkbey B, Mena E, Aras O, Garvey B, Grant K and Choyke PL. Functional and molecular imaging: applications for diagnosis and staging of localised prostate cancer. *Clin Oncol (R Coll Radiol)* 2013; 25: 451-460.
 - [7] Vourganti S, Rastinehad A, Yerram NK, Nix J, Volkin D, Hoang A, Turkbey B, Gupta GN, Kruecker J, Linehan WM, Choyke PL, Wood BJ and Pinto PA. Multiparametric magnetic resonance imaging and ultrasound fusion biopsy detect prostate cancer in patients with prior negative transrectal ultrasound biopsies. *J Urol* 2012; 188: 2152-2157.
 - [8] Roobol MJ and Carlsson SV. Risk stratification in prostate cancer screening. *Nat Rev Urol* 2013; 10: 38-48.
 - [9] Afshar-Oromieh A, Haberkorn U, Hadaschik B, Habl G, Eder M, Eisenhut M, Schlemmer HP and Roethke MC. PET/MRI with a (68)Ga-PS-MA ligand for the detection of prostate cancer. *Eur J Nucl Med Mol Imaging* 2014; 40: 1629-1630.
 - [10] Menzin AW, Loret de Mola JR, Bilker WB, Wheeler JE, Rubin SC and Feinberg RF. Identification of oncofetal fibronectin in patients with advanced epithelial ovarian cancer: detection in ascitic fluid and localization to primary sites and metastatic implants. *Cancer* 1998; 82: 152-158.
 - [11] Inufusa H, Nakamura M, Adachi T, Nakatani Y, Shindo K, Yasutomi M and Matsuura H. Localization of oncofetal and normal fibronectin in colorectal cancer. Correlation with histologic grade, liver metastasis, and prognosis. *Cancer* 1995; 75: 2802-2808.
 - [12] Freire-de-Lima L, Gelfenbeyn K, Ding Y, Mandel U, Clausen H, Handa K and Hakomori SI. Involvement of O-glycosylation defining oncofetal fibronectin in epithelial-mesenchymal transition process. *Proc Natl Acad Sci U S A* 2011; 108: 17690-17695.
 - [13] Giannoni E, Bianchini F, Masieri L, Serni S, Torre E, Calorini L and Chiarugi P. Reciprocal activation of prostate cancer cells and cancer-associated fibroblasts stimulates epithelial-mesenchymal transition and cancer stemness. *Cancer Res* 2010; 70: 6945-6956.
 - [14] Gao D, Vahdat LT, Wong S, Chang JC and Mittal V. Microenvironmental regulation of epithelial-mesenchymal transitions in cancer. *Cancer Res* 2012; 72: 4883-4889.
 - [15] Gupta S, Iljin K, Sara H, Mpindi JP, Mirtti T, Vainio P, Rantala J, Alanen K, Nees M and Kallioniemi O. FZD4 as a mediator of ERG oncogene-induced WNT signaling and epithelial-to-mesenchymal transition in human prostate cancer cells. *Cancer Res* 2010; 70: 6735-6745.
 - [16] Kong D, Banerjee S, Ahmad A, Li Y, Wang Z, Sethi S and Sarkar FH. Epithelial to mesenchymal transition is mechanistically linked with stem cell signatures in prostate cancer cells. *PLoS One* 2010; 5: e12445.
 - [17] Sonmez H, Suer S, Karaarslan I, Baloglu H and Kokoglu E. Tissue fibronectin levels of human prostatic cancer, as a tumor marker. *Cancer Biochem Biophys* 1995; 15: 107-110.
 - [18] Jankovic MM and Kosanovic MM. Fibronectin pattern in benign hyperplasia and cancer of the prostate. *Dis Markers* 2008; 25: 49-58.
 - [19] Suer S, Sonmez H, Karaarslan I, Baloglu H and Kokoglu E. Tissue sialic acid and fibronectin levels in human prostatic cancer. *Cancer Lett* 1996; 99: 135-137.
 - [20] Albrecht M, Renneberg H, Wennemuth G, Moschler O, Janssen M, Aumuller G and Konrad L. Fibronectin in human prostatic cells in vivo and in vitro: expression, distribution, and pathological significance. *Histochem Cell Biol* 1999; 112: 51-61.
 - [21] Wu X, Burden-Gulley SM, Yu GP, Tan M, Lindner D, Brady-Kalnay SM and Lu ZR. Synthesis and evaluation of a peptide targeted small molecular Gd-DOTA monoamide conjugate for MR molecular imaging of prostate cancer. *Bioconjug Chem* 2012; 23: 1548-1556.
 - [22] Pilch J, Brown DM, Komatsu M, Jarvinen TA, Yang M, Peters D, Hoffman RM and Ruoslahti E. Peptides selected for binding to clotted plasma accumulate in tumor stroma and wounds. *Proc Natl Acad Sci U S A* 2006; 103: 2800-2804.
 - [23] Agemy L, Sugahara KN, Kotamraju VR, Gujrati K, Girard OM, Kono Y, Mattrey RF, Park JH, Sailor MJ, Jimenez AI, Cativiela C, Zanuy D, Sayago FJ, Aleman C, Nussinov R and Ruoslahti E. Nanoparticle-induced vascular blockade in human prostate cancer. *Blood* 2010; 116: 2847-2856.
 - [24] Rohrer M, Bauer H, Mintorovitch J, Requardt M and Weinmann HJ. Comparison of magnetic properties of MRI contrast media solutions at different magnetic field strengths. *Invest Radiol* 2005; 40: 715-724.

- [25] Winter PM, Caruthers SD, Kassner A, Harris TD, Chinen LK, Allen JS, Lacy EK, Zhang H, Robertson JD, Wickline SA and Lanza GM. Molecular imaging of angiogenesis in nascent Vx-2 rabbit tumors using a novel alpha(nu)beta3-targeted nanoparticle and 1.5 tesla magnetic resonance imaging. *Cancer Res* 2003; 63: 5838-5843.
- [26] Liu Y, Chen Z, Liu C, Yu D, Lu Z and Zhang N. Gadolinium-loaded polymeric nanoparticles modified with Anti-VEGF as multifunctional MRI contrast agents for the diagnosis of liver cancer. *Biomaterials* 2011; 32: 5167-5176.
- [27] Erdogan S, Medarova ZO, Roby A, Moore A and Torchilin VP. Enhanced tumor MR imaging with gadolinium-loaded polychelating polymer-containing tumor-targeted liposomes. *J Magn Reson Imaging* 2008; 27: 574-580.
- [28] Konda SD, Wang S, Brechbiel M and Wiener EC. Biodistribution of a 153 Gd-folate dendrimer, generation = 4, in mice with folate-receptor positive and negative ovarian tumor xenografts. *Invest Radiol* 2002; 37: 199-204.
- [29] Thomsen HS and Marckmann P. Extracellular Gd-CA: differences in prevalence of NSF. *Eur J Radiol* 2008; 66: 180-183.
- [30] Perazella MA and Rodby RA. Gadolinium-induced nephrogenic systemic fibrosis in patients with kidney disease. *Am J Med* 2007; 120: 561-562.
- [31] Franano FN, Edwards WB, Welch MJ, Brechbiel MW, Gansow OA and Duncan JR. Biodistribution and metabolism of targeted and nontargeted protein-chelate-gadolinium complexes: evidence for gadolinium dissociation in vitro and in vivo. *Magn Reson Imaging* 1995; 13: 201-214.
- [32] Bryant LH Jr, Jordan EK, Bulte JW, Herynek V and Frank JA. Pharmacokinetics of a high-generation dendrimer-Gd-DOTA. *Acad Radiol* 2002; 9 Suppl 1: S29-33.
- [33] Wang SJ, Brechbiel M and Wiener EC. Characteristics of a new MRI contrast agent prepared from polypropyleneimine dendrimers, generation 2. *Invest Radiol* 2003; 38: 662-668.
- [34] Ye F, Wu X, Jeong EK, Jia Z, Yang T, Parker D and Lu ZR. A peptide targeted contrast agent specific to fibrin-fibronectin complexes for cancer molecular imaging with MRI. *Bioconjug Chem* 2008; 19: 2300-2303.
- [35] Tan M, Wu X, Jeong EK, Chen Q and Lu ZR. Peptide-targeted Nanoglobular Gd-DOTA monoamide conjugates for magnetic resonance cancer molecular imaging. *Biomacromolecules* 2010; 11: 754-761.
- [36] Karmali PP, Kotamraju VR, Kastantin M, Black M, Missirlis D, Tirrell M and Ruoslahti E. Targeting of albumin-embedded paclitaxel nanoparticles to tumors. *Nanomedicine* 2009; 5: 73-82.
- [37] Simberg D, Duza T, Park JH, Essler M, Pilch J, Zhang L, Derfus AM, Yang M, Hoffman RM, Bhatia S, Sailor MJ and Ruoslahti E. Biomimetic amplification of nanoparticle homing to tumors. *Proc Natl Acad Sci U S A* 2007; 104: 932-936.
- [38] Zhou Z, Wu X, Kresak A, Griswold M and Lu ZR. Peptide targeted tripod macrocyclic Gd(III) chelates for cancer molecular MRI. *Biomaterials* 2013; 34: 7683-7693.
- [39] Ye Z, Wu X, Tan M, Jesberger J, Grisworld M and Lu ZR. Synthesis and evaluation of a polydisulfide with Gd-DOTA monoamide side chains as a biodegradable macromolecular contrast agent for MR blood pool imaging. *Contrast Media Mol Imaging* 2013; 8: 220-228.